is misleading: it fails to capture the fact that there are two distinct peaks, i.e., two distinct types of behavior. For example, take any small region of space-time in the evolution of a random initial condition. Typically, this region is in one or the other domain. The value of ρ_1 in the region is not halfway between the densities of the two domains, it is simply one or the other. That is, there is no region in which the density of nonzero cells is $\rho_1 \approx 0.41$, the global average value. Excepting the domain wall regions, which do not play a dominant role in the average (though for other rules they could), there are only regions with a density of nonzero cells close to either $\rho_1 \approx 0.25$ or $\rho_1 \approx 0.63$.

The global estimates of entropy and complexity are misleading in another way. The globally averaged entropies $h_0(\Omega_t)$ and $h_1(\Omega_t)$ are greater than the corresponding values for either domain. This is because Ω_t contains subwords in both domains, as well as subwords containing domain walls. It is questionable whether the estimated values of the complexities $C_0(\Omega_t)$ and $C_1(\Omega_t)$ can be assigned any meaning at all, given the extremely fast growth of the global machine Ω_t as calculated by the FME algorithm. Again, the global machine describes *all* of the structure of the state space, including the evolution and interaction of all of the walls—which, as we will see below, can be extremely complex.

11.3 Difference Patterns and Plumes

Fig. 11.5 shows space-time plots of the difference patterns $\mathbf{\Delta}_t$ generated by states chosen randomly from three different sets: $\mathcal{L} = \mathcal{A}^N$ (fig. 11.5(a)), $\mathcal{L} = \Lambda^0$ (fig. 11.5(b)), and $\mathcal{L} = \Lambda^1$ (fig. 11.5(c)).

In each case, the evolution was on a lattice of size $N = 100$ with periodic boundary conditions, and the perturbed cell was located at $j = N/2$. Note that for each of these patterns, the maximum instantaneous rate at which the perturbation spreads in either direction is equal to the "speed of light" of this rule, $c = 2\ \mathrm{cells/iteration}$. However, beneath this spreading light cone, the patterns differ markedly. The difference pattern $\mathbf{\Delta}_t$ for $\mathrm{s}_0 \in \mathcal{A}^N$ shows an irregular, disordered structure, while the patterns for the domains Λ^0 and Λ^1 both have the same regular structure. The latter two are in fact identical to each other for all t. When every other cell in space is removed with a "decimation" transducer $\mathrm{T}_{\mathrm{decimate}}$, they are identical to the space-time diagram of the chaotic, linear elementary CA rule 90 with an initial condition consisting of a single nonzero cell. That is, for $\mathcal{L} = \Lambda^0$ or Λ^1,

$$\mathrm{T}_{\mathrm{decimate}}(\mathbf{\Delta}_t) = \Phi_{90}^t(0^*10^*) \tag{11.2}$$

The difference plumes $\left\langle \Delta_t^i \right\rangle_{\mathcal{L}}$, or average difference patterns, for the three ensembles $\mathcal{A}^N$, Λ^0, and Λ^1 are shown in figs. 11.6(a), 11.6(b), and 11.6(c), respectively. Each plume was calculated using a Monte Carlo sample of 1000 state pairs on a lattice of size $N = 100$, with the perturbation in cell $j = N/2$.

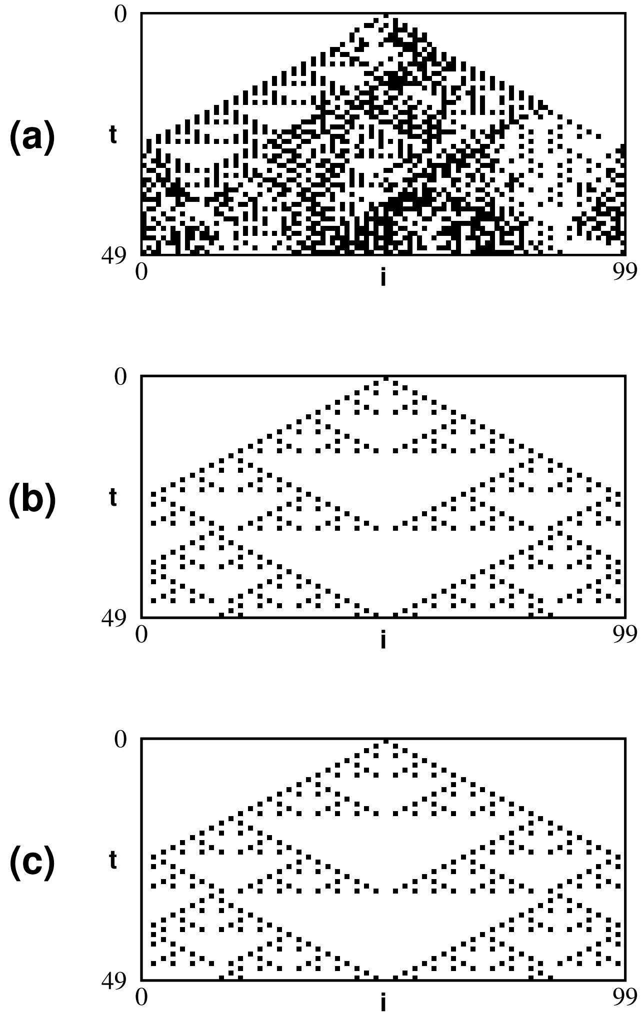

Fig. 11.5 Difference patterns $\mathbf{\Delta}_t$: (a) $\mathcal{L} = \mathcal{A}^N$. Global difference pattern in which the initial condition was randomly selected over the entire state space:$s_0 \in \mathcal{A}^N$; (b) random IC in domain $\mathcal{L} = \Lambda^0$; (c) random IC in domain $\mathcal{L} = \Lambda^1$. In each plot, evolution was on a lattice of size $N = 100$ and the initial condition was perturbed in cell $j = 50$. The patterns of (b) and (c) are identical, and are also identical to an "expanded" space-time diagram of elementary CA rule 90 in which a 0 is inserted between every horizontal pair of cells.

The difference plume for $\mathcal{A}^N$ (fig. 11.6(a)) is devoid of internal structure, with $\left\langle \Delta_t^i \right\rangle_{\mathcal{A}^N}$ smoothly decreasing toward the edges of the light cone. The plumes for Λ^0, and Λ^1 are quite different from this. In both of the latter, the averaged difference plume is identical to the difference pattern generated by a single initial condition. At each space-time point (i, t), $\left\langle \Delta_t^i \right\rangle_{\Lambda^0}$ is either zero or one. Thus all states in Λ^0 have the same difference pattern. The propagation of information is identical for all states in the ensemble. The situation is exactly the same for Λ^1, even though the two domains have strikingly different patterns. The important thing to note is that, without having identified the ensembles Λ^0 and Λ^1, we would never have noticed any structure in the difference plumes at all. The average over all of state space washes it out entirely.

The spatial "Lyapunov exponents" emphasize this difference. For both of the domains, λ_L and λ_R are evidently -2 and $+2$, respectively. On the other hand, the

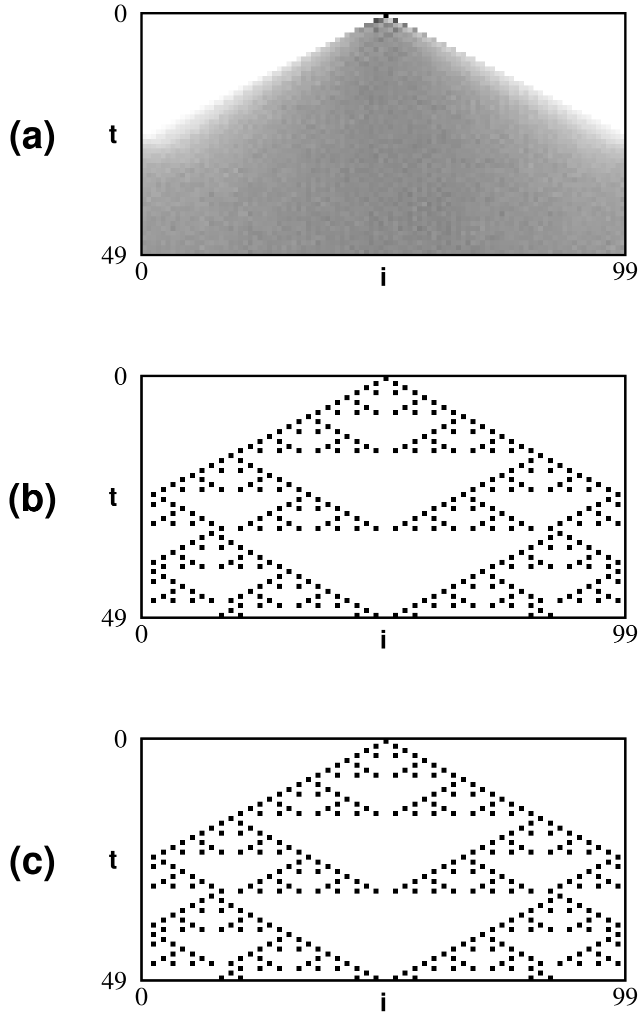

Fig. 11.6 Difference plumes $\langle \Delta_t^i \rangle_{\mathcal{L}}$: (a) $\mathcal{L} = \mathcal{A}^N$. Global difference plume averaged over initial conditions randomly selected over the entire state space; (b) initial conditions in domain $\mathcal{L} = \Lambda^0$; (c) initial conditions in domain $\mathcal{L} = \Lambda^1$. Note that while (a) appears to be a smooth surface, both (b) and (c) show structure. In fact, (b) and (c) are identical to the patterns of fig. 11.5(b) and 11.5(c). For each plot, $M = 1000$ pairs of states were iterated on a lattice of size $N = 100$. As above, each initial condition was perturbed in cell $j = 50$.

values for $\mathcal{A}^*$, shown in the last row of table 11.1, are $\lambda_{\mathrm{L}} = -1.64$ and $\lambda_{\mathrm{R}} = 1.73$. They were measured using an ensemble of $M = 1000$ pairs of states on a lattice of size $N = 1000$. For each pair, the left- and right-most cells in which the two states differed was recorded, and the average positions $\mu_L(t)$ and $\mu_R(t)$ over the ensemble were measured. Both of these quantities were plotted vs. time, and fit each curve to a polynomial, identifying λ_L and λ_R with the linear terms.

The third statistic associated with the difference plume is the volume $\zeta_{\mathcal{L}}(t)$. From fig. 11.6(a) it is clear that $\zeta_{\mathcal{A}^N}(t)$ increases smoothly with t, while $\zeta_{\Lambda^0}(t)$ and $\zeta_{\Lambda^1}(t)$ fluctuate in an orderly but discontinuous fashion. To further illustrate this point, fig. 11.7 shows a plot of $\zeta_{\mathcal{L}}(t)$ vs. t for $\mathcal{L} = \Lambda^0$ and $\mathcal{L} = \mathcal{A}^N$, with the same parameters as before. As expected, the curve of $\zeta_{\mathcal{A}^N}(t)$ vs. t (the dashed line) increases smoothly from $\zeta_{\mathcal{A}^N}(0) = 1$, with a very slight upward curvature. A least-squares fit to a power law form $\zeta_{\mathcal{A}^N}(t) = c_1 t^\alpha + c_2$ gives an exponent of $\alpha = 1.03$; alternatively, fitting $\zeta_{\mathcal{A}^N}(t)$ to a polynomial gives a linear slope of $m = 1.42$. The plot of $\zeta_{\Lambda^0}(t)$ vs. t, printed as a solid line, is quite different, however. All values of $\zeta_{\Lambda^0}(t)$ are powers of 2. Applying the above-mentioned relationship of the difference pattern $\mathbf{\Delta}_t$ and the evolution of a state with a single nonzero cell under ECA 90, we find the exact formula

$$\zeta_{\Lambda^0}(t) = 2^{\kappa(t)} \tag{11.3}$$

where $\kappa(n)$ is the number of 1s in the binary expansion of n.[103] Since the difference plumes for Λ^0 and Λ^1 are identical, so are the plume volumes: $\zeta_{\Lambda^1}(t) = \zeta_{\Lambda^0}(t)$ for all t.

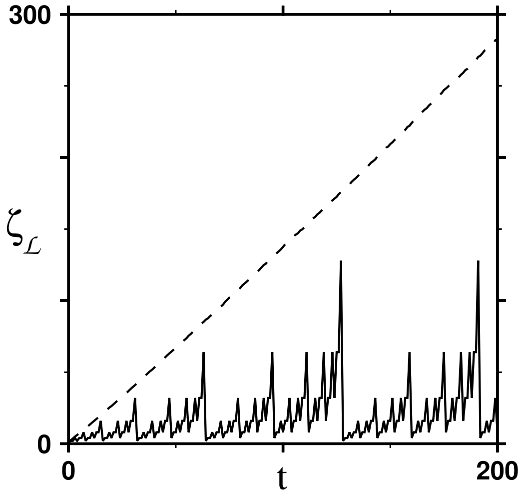

Fig. 11.7 Difference plume volumes $\zeta_{\mathcal{L}}(t)$ vs. t for the entire state space $\mathcal{L} = \mathcal{A}^N$ (dashed line) and for domain $\mathcal{L} = \Lambda^0$ (solid line). The plume volume for the other domain, $\mathcal{L} = \Lambda^1$, is identical to $\zeta_{\Lambda^0}(t)$.

11.4 Domain Interfaces

Having identified the regular domains Λ^0 and Λ^1 and measured their properties, it is natural to turn next to the study of the interface between two adjacent domains. This section gives a brief survey of the temporal evolution of states consisting of two domains laid side-by-side, focusing on the region where they meet. We make no attempt at a complete characterization, but merely indicate the starting point. Our purpose is to illustrate the utility of analyzing the state space in terms of the pattern bases: i.e., to show how knowledge of the domains gives a new systematic view of the variety of the space-time structures—walls, dislocations, and (possibly) "particles"—that a spatial system can generate.

We are concerned here with the behavior of states initially consisting of two concatenated domains Λ^i and Λ^j, with the wall between the two at a given cell m. Each domain has a specific phase, but is otherwise chosen at random. As before, ensembles of such "two-domain" states are denoted by $\Lambda^{i,j}$. The state is then allowed to evolve, and the structure of the interface between the domains is analyzed. On a finite lattice, the periodic boundary conditions create another wall at cell 0, but in our investigations we will be using sufficiently large lattices that this second wall can be ignored over the time interval of our measurements.

For the two domains we are studying, we have the range of relative phases $\delta\phi^{00} \in \{-1, 0, 1\}$, $\delta\phi^{01} \in \{-1, ..., 3\}$, $\delta\phi^{01} \in \{-3, ..., 1\}$, and $\delta\phi^{11} \in \{-3, ..., 3\}$. Note that a state in $\Lambda^{i,i}$ with $\delta\phi^{ii} = 0$ does not in fact contain a wall, since the two parts of the state have the same domain type and same phase at the junction. However, for states in $\Lambda^{i,j}$ with $i \neq j$, there is a wall for all values of $\delta\phi^{ij}$, including $\delta\phi^{ij} = 0$.

Because the machines for the domains are cyclic—i.e., the machine states are visited in cyclic order—many of the relative phases are degenerate; for example, $\Lambda^{0,0}$ with $\delta\phi^{00} = +1$ is identical to $\Lambda^{0,0}$ with $\delta\phi^{00} = -1$. Similar degeneracies occur for the other $\Lambda^{i,j}$ as well. The net result is that the number of distinct interface types is reduced to eight, which are listed below.

Interface plots

Filtered space-time plots of six randomly selected two-domain states, representing six of the eight possible combinations of domains and relative phases, are shown in fig. 11.8. Examples of all four possible domain pairs $\Lambda^{i,j}$ are shown, and in addition we show two examples each of $\Lambda^{1,0}$ and $\Lambda^{1,1}$, with different values of $\delta\phi$, to investigate the importance of the relative phase. Reading the figure from left to right, top to bottom, they are (a) $\Lambda^{0,0}$ with relative phase $\delta\phi^{00} = 1$, (b) $\Lambda^{0,1}$ with $\delta\phi^{01} = 0$, (c) $\Lambda^{1,0}$ with $\delta\phi^{10} = 0$ (d) $\Lambda^{1,0}$ with $\delta\phi^{10} = 1$, (e) $\Lambda^{1,1}$ with $\delta\phi^{11} = 1$, and (f) $\Lambda^{1,1}$ with $\delta\phi^{11} = -1$. The two remaining interface types not shown are (g) $\Lambda^{0,1}$ with $\delta\phi^{01} = 1$ and (h) $\Lambda^{1,1}$ with $\delta\phi^{11} = 2$, for which the wall evolution is quite similar to that of interfaces (a) and (e), respectively. Cells in Λ^{0} are shown in white, cells in Λ^{1} are gray, and all walls are black. The lattice size is $N = 1000$, of which only the central portion is displayed. Each state starts out at $t = 0$ with a single wall at cell $m = 500$.

Perhaps the most obvious feature of the plots in fig. 11.8 is that behavior of the interface can vary widely depending on the domains to either side. In the roughest approximation, there are two qualitatively different types of evolution: (i) spreading interface, and (ii) localized drift.

In figs. 11.8(a), 11.8(b) and 11.8(e), the number of walls is plainly not conserved. The single wall at $t = 0$ splits into a whole population of walls that move about, annihilate each other, and themselves split into multiple offspring. The interfacial region, i.e. the region in which walls are present, spreads rapidly to either side. In these plots, the identification of walls as “particles” is problematic at best, since the interfaces do not possess even the most basic attribute of particles, spatial localization.

In figs. 11.8(c), 11.8(d), and 11.8(f), on the other hand, the interfacial region remains localized in space, and drifts as a whole in one direction or another. The number of walls fluctuates but does not blow up as in the other plots. From time to time, a single wall does split into multiple offspring, but these offspring are quickly

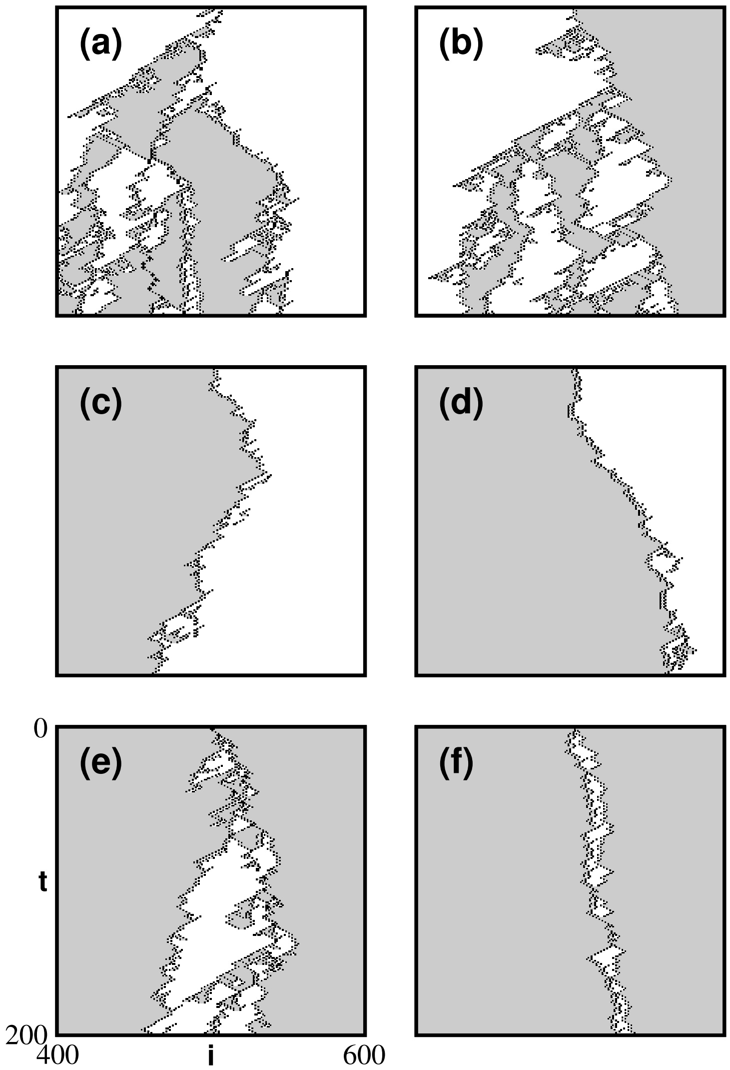

Fig. 11.8 Evolution of domain interfaces. Each state starts out with a single wall at cell $j = 500$. The initial conditions were chosen randomly from the following ensembles: (a) $\Lambda^{0,0}$ with relative phase $\delta\phi^{00} = 1$; (b) $\Lambda^{0,1}$ with $\delta\phi^{01} = 0$; (c) $\Lambda^{1,0}$ with $\delta\phi^{10} = 0$; (d) $\Lambda^{1,0}$ with $\delta\phi^{10} = 1$; (e) $\Lambda^{1,1}$ with $\delta\phi^{11} = 1$; and (f) $\Lambda^{1,1}$ with $\delta\phi^{11} = -1$. Cells in the interior of Λ^0 are shown in white, cells in Λ^1 are gray, and all walls are black.

annihilated. These interfaces behave as localized "real" particles surrounded by a cloud of interacting "virtual" particles.

The diffusive character of wall motion is also immediately apparent. The walls in each plot appear to be following some type of random walk, with or without a net drift. This statement will be made more quantitative in the next subsection.

The dependence on relative phase is illustrated in figs. 11.8(e) and (f). Both plots start with a state in $\Lambda^{1,1}$, but the relative phase differs. In fig. 11.8(e), with $\delta\phi^{11} = 1$, the interface spreads; whereas in fig. 11.8(f), with $\delta\phi^{11} = -1$, it remains localized.

Interface plumes

The plots in fig. 11.8 show only a single state in each of their respective ensembles.